Biophysical Journal
Article

Biophysical Society

Active Prestress Leads to an Apparent Stiffening of Cells through Geometrical Effects

Elisabeth Fischer-Friedrich[1,*]
[1]Biotechnology Center, Technische Universität Dresden, Dresden, Germany

ABSTRACT Tuning of active prestress, e.g., through activity of molecular motors, constitutes a powerful cellular tool to adjust cellular stiffness through nonlinear material properties. Understanding this tool is an important prerequisite for our comprehension of cellular force response, cell shape dynamics, and tissue organization. Experimental data obtained from cell-mechanical measurements often show a simple linear dependence between mechanical prestress and measured differential elastic moduli. Although these experimental findings could point to stress-induced structural changes in the material, we propose a surprisingly simple alternative explanation in a theoretical study. We show how geometrical effects can give rise to increased cellular force response of cells in the presence of active prestress. The associated effective stress-stiffening is disconnected from actual stress-induced changes of the elastic modulus, and should therefore be regarded as an apparent stiffening of the material. We argue that new approaches in experimental design are necessary to separate this apparent stress-stiffening due to geometrical effects from actual nonlinearities of the elastic modulus in prestressed cellular material.

INTRODUCTION

Cells need to deform themselves during many physiological processes in the body, such as cell division, cell migration, or the complex events of morphogenesis. To understand dynamic cell deformation from a physical point of view, we need to quantify cell material properties and its active regulation through the underlying molecular cell biology. Cells are a complex viscoelastic material whose material properties are timescale-dependent and nonlinear beyond strains of a few percent (1). Mechanical stress therefore alters cell-mechanical properties, making cells stiffer or softer (1–5). The material properties of a cell are mainly determined by its cytoskeleton. Intriguingly, cells are able to self-tune the mechanical prestress in the cytoskeleton through the action of molecular motors, giving the cell a tool to actively regulate its material stiffness through dynamic adjustment of active prestress together with stress-stiffening or stress-softening. Many studies report stress-stiffening through active prestress (1,6–10); however, opposite findings of cell-softening have also been reported (11). Stiffness modulation through the action of motor proteins in actin meshworks was further corroborated by in vitro measurements (12–14). It has been suggested that cytoskeletal stress-stiffening may be understood in terms of the nonlinear entropic thermal stretch modulus of a single polymer (15–17) or the stress-induced "pull-out" of soft bending modes and a transition toward a stretch-dominated regime (18). As a third option, load-dependent binding dynamics of actin cross-linkers has been suggested (19). Entropic effects predict a power law scaling of $3/2$ for the resulting differential shear modulus (16), the pull-out of soft bending modes gives rise to a power law scaling between $1/2$ and 1 (18). Furthermore, linear stress-stiffening has been reported for marginal networks (20,21) and for tensegrity models (22).

Experimental data obtained from cell-mechanical measurements often show a linear dependence between measured differential elastic moduli and active mechanical prestress. This corresponds to a power law with exponent one in dependence of prestress (1,6–8). Although these experimental findings could point to complex structural changes of the cytoskeleton through active prestress and accordant modification of its elastic modulus, we propose a surprisingly simple alternative explanation: pure geometrical effects may give rise to an increased force response and thus an effective stiffening of actively prestressed material. Associated effective stiffening is, however, independent of actual stress-dependent changes of the elastic modulus as a material parameter of the cytoskeleton in a coarse-grained continuum description. Thus the associated stiffening will be denoted as "apparent stiffening." We will discuss two different geometrical effects: 1) stress-stiffening through geometrical-coupling, and 2) shear-induced

Submitted June 14, 2017, and accepted for publication November 14, 2017.
*Correspondence: elisabeth.fischer-friedrich@tu-dresden.de
Editor: David Piston.
https://doi.org/10.1016/j.bpj.2017.11.014

nematic alignment. In fact, when present, these effects disguise the actual stress-dependence of the elastic modulus and may partly account for incoherences in the cell mechanics field, such as order of magnitude differences in measured shear moduli and contradicting trends (stiffening or softening) in response to mechanical prestress.

Apparent stress-stiffening through geometrical coupling

In the following paragraphs, we discuss two simplified examples of cell-mechanical probing to illustrate the general phenomenon of apparent stress-stiffening through geometrical coupling in adherent and nonadherent cells. In our calculations, we will henceforth assume that displacements and strains are small. We will thus follow the approach of linear elasticity theory, keeping only terms to first order in strain and deformation.

Deformation of an adhered model cell. We will first consider the case of a one-dimensional, actively prestressed fiber tethered to a substrate as a minimal model of an adherent cell. Consider the experimental scenario sketched in Fig. 1 *A*, where the fiber center is oscillated around a mean height with $h(t) = h_0 + \tilde{h}\exp(i\omega t)$ through a force exerted by an adherent bead. The one-dimensional stress in the fiber has a contribution from active prestress $\sigma_{\rm act}$ and a deformation-induced viscoelastic contribution (8):

$$\sigma(t) \;=\; \sigma_{\rm act} + G^*(\sigma_{\rm act},\omega)\epsilon(t), \tag{1}$$

where $G^*(\sigma_{\rm act},\omega)$ is the prestress- and frequency-dependent complex elastic modulus of the fiber, $\epsilon(t) = \tilde{\epsilon}\exp(i\omega t)$ is the strain with respect to fiber length changes, and $\omega = 2\pi f$ is the angular frequency of the applied oscillation.

The measured force signal is

$$F(t) \;=\; g(t)(\sigma_{\rm act} + G^*(\sigma_{\rm act},\omega)\epsilon(t)), \tag{2}$$

where $\alpha(t)$ is the angle between the fiber and the substrate (see Fig. 1 *A*) and $g(t) = 2\sin\alpha(t)$ is a time-dependent geometrical factor. We make the ansatz

$$g(t) \;=\; g_0 + \tilde{g}\exp(i\omega t), \tag{3}$$

$$F(t) \;=\; F_0 + \tilde{F}\exp(i\omega t), \tag{4}$$

where g_0 and F_0 are average values of the geometrical factor and measured force, respectively, whereas $\tilde{g}$ and $\tilde{F}$ characterize emerging oscillatory changes. Here, $\tilde{F}$ may take complex values if the respective force oscillations are not in phase with the imposed oscillations of bead height. We find to first order

$$F(t) \;=\; F_0 + (\tilde{g}\sigma_{\rm act} + g_0 G^*(\sigma_{\rm act},\omega)\tilde{\epsilon})\exp(i\omega t). \tag{5}$$

Force oscillation amplitudes thus contain a contribution $\tilde{g}\sigma_{\rm act}$ proportional to the active prestress if the oscillation amplitude of the geometrical factor g does not vanish. We will denote this effect as geometrical coupling of active prestress into the force signal. In a conventional rheological analysis that disregards the presence of active prestress, the force amplitude is assumed to scale with the complex elastic modulus of the system for a given strain. Therefore, the effective elastic modulus would be determined to scale as

$$G^*_{\rm eff}(\sigma_{\rm act},\omega) \propto \frac{1}{g_0}\frac{\tilde{g}}{\tilde{\epsilon}}\sigma_{\rm act} + G^*(\sigma_{\rm act},\omega). \tag{6}$$

A short calculation yields (see Supporting Material)

$$\frac{1}{g_0}\frac{\tilde{g}}{\tilde{\epsilon}} = \frac{L^2}{4h_0^2}, \tag{7}$$

where L is the fiber length in a straight conformation (see Fig. 1 *A*). Thus, the effective shear modulus shows apparent linear stress-stiffening, with a slope proportional to $L^2/(4h_0^2)$ and an additional active contribution $1/g_0 \times \tilde{g}/\tilde{\epsilon} \times \sigma_{\rm act}$. In particular, for sufficiently small values of mean height h_0, the active contribution starts to override the contribution of the actual complex elastic modulus in the measurement and the slope of the apparent stress-stiffening can, in principle, become arbitrarily large.

In the above example, geometrical coupling of active prestress has contributed only a constant term to the effective storage modulus of the system because the deformation

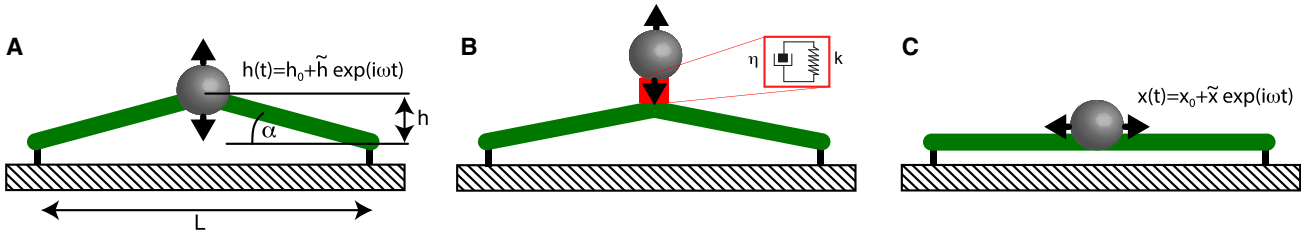

FIGURE 1 Different setups for rheological probing of a contractile cytoskeletal fiber. The force response of the fiber is affected by the magnitude of inherent active prestress in measurement scenarios (*A*) and (*B*). In setup (*C*), contributions of active prestress to force oscillations are avoided. To see this figure in color, go online.

and the geometrical factor were in phase. However, in general, out-of-phase oscillations of the geometrical factor are possible, e.g., in the case of a prestressed material coupled to a viscoelastic connector (see Fig. 1 *B*; Supporting Material). If an attached bead is deflected horizontally along the fiber (see Fig. 1 *C*), active contributions to the force oscillations are avoided and we have $G^*_{\mathrm{eff}}(\sigma_{\mathrm{act}},\omega) = G^*(\sigma_{\mathrm{act}},\omega)$.

Deformation of a nonadherent model cell. As a second example, we consider a nonadherent cell that is being probed in a parallel plate assay subject to oscillatory height changes $h(t) = h_0 + \tilde{h}\exp(i\omega t)$ (see Fig. 2 *A*). Accordant measurements were performed on mitotic cells in (8). We will regard the cell as a liquid-filled pressurized shell, where the shell material is constituted by the plasma membrane and the neighboring actomyosin cortex. To keep our calculations simple, we will assume that the deformation-induced stress in the cortex-membrane layer is a spatially homogeneous, isotropic, in-plane stress governed by an area dilation modulus and an active mechanical prestress σ_{act}. Furthermore, we will assume that viscous contributions of the cytoplasm are negligible (8). With these simplifications, Laplace's law $\Delta p = 2H\sigma$ holds at all times for the free-cell surface area, where H denotes the mean curvature of the cell surface, σ is the two-dimensional mechanical stress in the cortical shell, and Δp is a balancing pressure excess in the cytoplasm (23). Analogous to the previous example, we have

$$F(t) \;=\; g(t)\big(\sigma_{\mathrm{act}} + K^*_A(\sigma_{\mathrm{act}},\omega)\epsilon_A(t)\big), \tag{8}$$

where $g(t)$ is again a geometrical factor, $K^*_A(\sigma_{\mathrm{act}},\omega)$ is the prestress- and frequency-dependent complex area dilation modulus, and $\epsilon_A(t) = \tilde{\epsilon}_A\exp(i\omega t)$ is the corresponding surface area shear with amplitude $\tilde{\epsilon}_A$. If the cell is not adhering to the contacting plate, we have a vanishing contact angle and thus, according to Laplace's law, $g(t) = 2A_{\mathrm{con}}(t)H(t)$, where $A_{\mathrm{con}}(t)$ denotes the time-variable contact area of the cell-plate interface. Due to Laplace's law, the oscillatory variations of the geometrical factor are in phase with surface area oscillations such that $\tilde{g}$ is real. We find analogous to Eq. 6,

$$\tilde{F} \propto K^*_{A,\mathrm{eff}}(\sigma_{\mathrm{act}},\omega) \propto \frac{1}{g_0}\frac{\tilde{g}}{\tilde{\epsilon}_A}\sigma_{\mathrm{act}} + K^*_A(\sigma_{\mathrm{act}},\omega). \tag{9}$$

Thus, the effective modulus $K^*_{A,\mathrm{eff}}(\sigma_{\mathrm{act}},\omega)$ contains a term linear in active prestress giving rise to an (apparent) linear stress-stiffening, in addition to possible actual stress-stiffening of the material given by the explicit dependence of $K^*_A(\sigma_{\mathrm{act}},\omega)$ on σ_{act}. To illustrate the magnitude of this apparent linear stress-stiffening, we estimated the stiffening slope $1/g_0 \times \tilde{g}/\tilde{\epsilon}_A$ for a cell subject to different degrees of confinement, as described in (8). It is noteworthy that the stiffening slope $1/g_0 \times \tilde{g}/\tilde{\epsilon}_A$ is independent of the strain amplitude $\tilde{\epsilon}_A$ and may take arbitrarily large values as it diverges for large cell confinement heights (see Fig. 2 *B*).

In conclusion, the two examples presented above show that geometrical coupling may give rise to an apparent linear stress-stiffening during cell-mechanical measurements with stiffening slopes that depend crucially on the chosen measurement setup. Therefore, the associated stiffening slopes are no material parameters.

Apparent stress-stiffening through shear-induced nematic alignment

So far, we have considered examples of cell-mechanical probing where no shear deformations have been involved. Typically, shear deformations do, however, play a role and give rise to an additional form of apparent linear stress-stiffening through geometrical effects. Stiffening through fiber alignment and active prestress has already been discussed in previous works (5,24). We reformulate it here in the continuum mechanics framework of active gel theory.

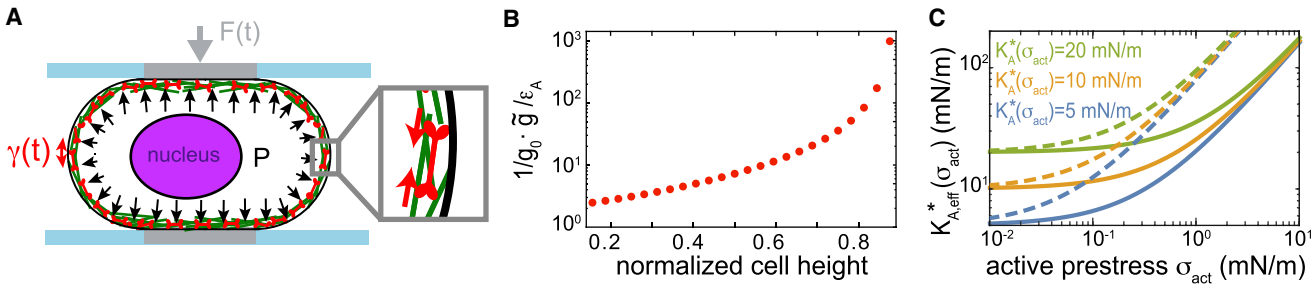

FIGURE 2 Oscillatory parallel plate confinement of non-adherent cells. (*A*) Cells are uniaxially compressed between parallel plates oscillating around a mean confinement height h_0. Cortical contractility of the cell is balanced by an internal hydrostatic pressure excess. During the oscillation cycle, cell contact area and curvature of the free-cell surface change, as well as the internal pressure and the mechanical stress in the outer cortex-membrane layer. (*B*) Apparent stress-stiffening slope $1/g_0 \times \tilde{g}/\tilde{\epsilon}_A$ in dependence of average cell confinement height, normalized by the cell diameter in a spherical conformation, is shown. (*C*) Apparent modulus $K^*_{A,\mathrm{eff}}(\sigma_{\mathrm{act}})$ calculated according to the right hand side of Eq. 9 for a cell confined to a normalized cell height of 0.65 (*solid lines*) and 0.8 (*dashed lines*) is shown. The actual area dilation modulus $K^*_A(\sigma_{\mathrm{act}})$ was chosen to be constant and thus stress-independent. Parameters were motivated by measurements of mitotic cells (8). To see this figure in color, go online.

Furthermore, we incorporate it as a new aspect of the effect of filament turnover. Nematic alignment of cytoskeletal polymers has been discussed before in the case of viscous flows in active gels (25) but has, to our knowledge, not yet been explicitly connected to stress-stiffening in cells.

In the following, we discuss how shear deformations change the nematic order of a polymer network leading to an apparent linear stiffening in the presence of active prestress. For simplicity, we discuss a two-dimensional material. In this case, the nematic order tensor is defined as

$$\mathbf{Q} = \int_0^{2\pi} \begin{pmatrix} \cos(\varphi)^2 - \frac{1}{2} & \cos(\varphi)\sin(\varphi) \\ \cos(\varphi)\sin(\varphi) & \sin(\varphi)^2 - \frac{1}{2} \end{pmatrix} p(\varphi)\mathrm{d}\varphi, \quad (10)$$

where $p(\varphi)$ is the probability distribution of finding a polymer with an orientation of polar angle φ. We will assume that the network is isotropic in the reference configuration and $p(\varphi) = 1/(2\pi)$. Thus, before deformation, $\mathbf{Q} = 0$. After application of an affine shear deformation to an area element, this orientation distribution will be changed (see Fig. 3 *A*). To illustrate that, consider a small homogeneous shear whose principal axes are, without loss of generality, in x–y direction. The associated strain tensor reads

$$\epsilon = \begin{pmatrix} \lambda & 0 \\ 0 & -\lambda \end{pmatrix}. \quad (11)$$

In this case, a polymer orientation φ will on average be realigned by the mapping $\varphi \to \varphi - 2\lambda\cos(\varphi)\sin(\varphi)$ to first order in λ, leading to a new probability distribution $p'(\varphi) = 1/2\pi + \cos(2\varphi)\lambda/\pi$. In this way, polymer orientations along the x axis become more likely (see Fig. 3). As a consequence, the active prestress becomes anisotropic. Using Eq. 10, the nematic order tensor is to first order in strain $\mathbf{Q} = \epsilon/2$. Following active gel theory (26), we make the ansatz

$$\sigma^{\mathrm{act}}(\epsilon) = \zeta_1 \Delta\mu\, 1 + \zeta_2 \Delta\mu \mathbf{Q}(\epsilon), \quad (12)$$

for active prestress in the cytoskeleton, where $\Delta\mu$ denotes the difference between the chemical potentials of ATP and its hydrolysis products. If the material is elastic with prestress-dependent shear modulus $G(\sigma_{\mathrm{act}})$, the overall traceless stress after a shear deformation is thus

$$2\left(\frac{\zeta_2}{8\zeta_1}\sigma_{ii}^{\mathrm{act}}(0) + G(\sigma_{\mathrm{act}})\right)\epsilon. \quad (13)$$

Therefore, in an analysis of the force response that does not compensate for the influence of active prestress, the effective shear modulus would thus be identified as

$$G_{\mathrm{eff}}(\sigma_{\mathrm{act}}) = \frac{\zeta_2}{8\zeta_1}\sigma_{ii}^{\mathrm{act}}(0) + G(\sigma_{\mathrm{act}}). \quad (14)$$

Since the cytoskeleton turns over through depolymerization and repolymerization processes, induced nematic alignment may be lost over time with the original polymer orientation distribution being reestablished. In the following, we will adapt our above considerations on shear-induced nematic alignment to a viscoelastic material. Adopting the scheme in Reymann et al. (25), we will assume that the material turnover takes place on a time scale τ_{to} and that Maxwell-type dynamics governs the time dependence of the nematic order tensor such that $\dot{\mathbf{Q}} = \dot{\epsilon}/2 - \mathbf{Q}/\tau_{to}$. In Fourier space, we obtain, correspondingly,

$$\mathbf{Q}(\omega) = \frac{i\omega}{(i\omega + 1/\tau_{to})}\frac{\epsilon(\omega)}{2}, \quad (15)$$

thus

$$G^*_{\mathrm{eff}}(\sigma_{\mathrm{act}}, \omega) = \frac{\zeta_2}{8\zeta_1}\sigma_{ii}^{\mathrm{act}}(0)\frac{i\omega}{(i\omega + 1/\tau_{to})} + G^*(\sigma_{\mathrm{act}}, \omega), \quad (16)$$

which includes a term proportional to active prestress in addition to the actual shear modulus. For a homogeneous

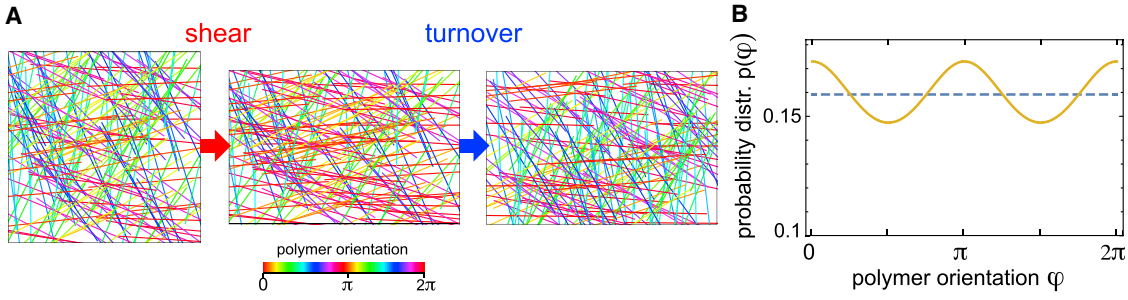

FIGURE 3 Nematic alignment through shear. (*A*) Randomly oriented polymer rods (*left panel*) are reoriented by a shear deformation with $\lambda = 0.2$. Shear deformations induce nematic alignment of biopolymers leading to a deformation-resistance proportional to active prestress (*middle panel*). Turnover reestablishes the original orientation distribution of polymers (*right panel*). The color legend indicates the orientation angle φ of polymers of different color. (*B*) Polymer distribution before (*dashed line*) and after (*solid line*) shear deformation with $\lambda = 0.2$. To see this figure in color, go online.

shear in a three-dimensional material, a corresponding calculation gives

$$G^*_{\mathrm{eff}}(\sigma_{\mathrm{act}},\omega) = \frac{\zeta_2}{15\zeta_1}\sigma^{\mathrm{act}}_{ii}(0)\frac{i\omega}{(i\omega+1/\tau_{to})} + G^*(\sigma_{\mathrm{act}},\omega). \tag{17}$$

The expected stress-stiffening slope of the effective storage modulus due to nematic alignment is proportional to ζ_2/ζ_1. As the parameters ζ_1 and ζ_2 are a priori not known, the magnitude of the associated stress-stiffening slope is not entirely clear. A simple consideration gives an order of magnitude estimate; if polymers of different orientation in the cytoskeletal network do not interact to generate active prestress, active prestress is proportional to the averaged tensor product of filament orientations and we have $\zeta_1 = \zeta_2/2$ in two dimensions ($\zeta_1 = \zeta_2/3$ in three dimensions). Thus, the associated stress-stiffening slope would be $1/2$ ($3/5$ in three dimensions). It is noteworthy that shear-induced nematic alignment will influence material properties also in the absence of active prestress. However, in this case, effects of nematic alignment and emergent anisotropies on the force response are second order in strain and thus negligible for small deformations (27). Only in the presence of active prestress, these effects become first order and non-negligible.

DISCUSSION

We have presented theoretical considerations that predict cellular force response to scale linearly with active mechanical prestress in the absence of actual nonlinear material properties (i.e., if $\mathrm{d}G^*(\sigma_{\mathrm{act}})/\mathrm{d}\sigma_{\mathrm{act}} = 0$). The resulting apparent stress-stiffening roots in an increase of measured force amplitudes due to geometrical coupling of active prestress and/or shear-induced nematic alignment of the underlying polymer network during dynamic deformation of the cellular material. In particular, geometrical coupling may change effective cell moduli in the presence of cytoskeletal contractility (= active prestress) by orders of magnitude depending on the choice of measurement parameters (see Fig. 2). This phenomenon may contribute to the puzzling diversity of cell mechanical moduli reported in the literature (28). Stress-stiffening through active prestress in cells has been shown before in several experimental studies, with mainly linear stiffening trends and slopes between 0.2 and 45 (see Table 1) (6–8,24,29,30). An influence of geometrical coupling or shear-induced nematic alignment on previously reported stress-stiffening slopes is conceivable.

If the geometrical factor of geometrical coupling is changing in phase with applied strain during the measurement, geometrical coupling gives merely rise to a frequency-independent addition to the effective storage modulus. If the actual storage modulus approaches zero at small frequencies, the active prestress contribution may thus be identified as $G'_{\mathrm{eff}}(\sigma_{\mathrm{act}},\omega\to 0)$. If the coupling geometrical factor can be estimated, this offers the chance to measure both the complex elastic modulus and the active prestress jointly from one rheological measurement. To this end, the oscillatory force signal needs to be divided by the time-dependent geometrical factor to obtain a stress signal for rheological analysis (see also Fischer-Friedrich et al. (8)). The resulting modulus is then the actual elastic modulus of the material. On the other hand, dividing the baseline force F_0 by the time-averaged geometrical factor g_0 yields the active prestress. In some ideal measurement setups, geometrical coupling can be entirely avoided (see Fig. 2 *C*). However, such setups are not easily experimentally realized.

Shear-induced nematic alignment generates a frequency-dependent apparent stiffening of actively prestressed material. However, resulting apparent stress-stiffening is independent of the measurement method and thus a true material parameter. Thus, disentangling the active stiffness contribution from the actual passive modulus might not even considered to be necessary. Many measurements report cell rheology which exhibits diverging moduli at high frequencies and short timescales (1,31). As active stiffness contributions through shear-induced nematic alignment are bounded by $\zeta_2/\zeta_1\sigma^{\mathrm{act}}_{ii}(0)$, they are expected to give negligible contributions to an effective elastic modulus at large frequencies.

It is likely that the geometrical stress-stiffening effects described here may also contribute to nonlinear mechanics of cells in the presence of external mechanical prestress. However, exertion of a constant external prestress to viscoelastic cellular material leads, in general, to large deformations (e.g., through a constant strain rate in a rheometer) and large inherent anisotropies of the material. Both effects

TABLE 1 Summary of Previously Measured Stress-Stiffening of Cells in Response to Active Prestress

Reference	Method	Approximate Stiffening Slope	Cells
Wang et al. (6), Stamenović et al. (24)	magnetic twisting cytometry and traction force microscopy	≈0.2	adhered HASM cells
Stamenović et al. (7)	magnetic twisting cytometry and traction force microscopy	≈3 to 6.6, for $f = 0.1$ to 1000 Hz	adhered HASM cells
Kollmannsberger et al. (29)	magnetic tweezer	1.68	adhered, several cell lines
Fischer-Friedrich et al. (8)	AFM cell confinement	33 and 45, for $f = 0.1$ and 1 Hz	suspended, mitotic HeLa cells

AFM, atomic force microscopy; HASM, human airway smooth muscle.

further complicate a theoretical description considerably. Our results indicate that effective elastic moduli may become entirely determined by active prestress for sufficiently large values of prestress. In the context of external prestress, this could provide an alternative explanation for the recent finding of externally prestressed collagen networks whose shear moduli were found to be collagen concentration independent at sufficiently large mechanical loadings (21).

In summary, our findings show that geometrical effects may disguise the actual stress-dependence of cellular elastic moduli during cell-mechanical measurements in the presence of active prestress. New approaches in experimental design are necessary to separate apparent stiffening from actual stress-induced stiffening or softening of cells.

SUPPORTING MATERIAL

Supporting Materials and Methods are available at http://www.biophysj.org/biophysj/supplemental/S0006-3495(17)31243-2.

AUTHOR CONTRIBUTIONS

E.F.-F. developed the theoretical analysis and wrote the manuscript.

ACKNOWLEDGMENTS

I thank Benjamin Friedrich, Stefan Münster, and Ben Fabry for discussions on the topic and critical reading of the manuscript.

REFERENCES

1. Kollmannsberger, P., and B. Fabry. 2011. Linear and nonlinear rheology of living cells. *Annu. Rev. Mater. Res.* 41:75–97.
2. Kollmannsberger, P., and B. Fabry. 2009. Active soft glassy rheology of adherent cells. *Soft Matter.* 5:1771–1774.
3. Lange, J. R., C. Metzner, …, B. Fabry. 2017. Unbiased high-precision cell mechanical measurements with microconstrictions. *Biophys. J.* 112:1472–1480.
4. Stricker, J., T. Falzone, and M. L. Gardel. 2010. Mechanics of the F-actin cytoskeleton. *J. Biomech.* 43:9–14.
5. Ingber, D. E., N. Wang, and D. Stamenović. 2014. Tensegrity, cellular biophysics, and the mechanics of living systems. *Rep. Prog. Phys.* 77:046603.
6. Wang, N., I. M. Tolić-Nørrelykke, …, D. Stamenović. 2002. Cell prestress. I. Stiffness and prestress are closely associated in adherent contractile cells. *Am. J. Physiol. Cell Physiol.* 282:C606–C616.
7. Stamenović, D., B. Suki, …, J. J. Fredberg. 2004. Rheology of airway smooth muscle cells is associated with cytoskeletal contractile stress. *J. Appl. Physiol.* 96:1600–1605.
8. Fischer-Friedrich, E., Y. Toyoda, …, F. Jülicher. 2016. Rheology of the active cell cortex in mitosis. *Biophys. J.* 111:589–600.
9. Fernández, P., P. A. Pullarkat, and A. Ott. 2006. A master relation defines the nonlinear viscoelasticity of single fibroblasts. *Biophys. J.* 90:3796–3805.
10. Jansen, K. A., R. G. Bacabac, …, G. H. Koenderink. 2013. Cells actively stiffen fibrin networks by generating contractile stress. *Biophys. J.* 105:2240–2251.
11. Chan, C. J., A. E. Ekpenyong, …, F. Lautenschläger. 2015. Myosin II activity softens cells in suspension. *Biophys. J.* 108:1856–1869.
12. Mizuno, D., C. Tardin, …, F. C. Mackintosh. 2007. Nonequilibrium mechanics of active cytoskeletal networks. *Science.* 315:370–373.
13. Bendix, P. M., G. H. Koenderink, …, D. A. Weitz. 2008. A quantitative analysis of contractility in active cytoskeletal protein networks. *Biophys. J.* 94:3126–3136.
14. Koenderink, G. H., Z. Dogic, …, D. A. Weitz. 2009. An active biopolymer network controlled by molecular motors. *Proc. Natl. Acad. Sci. USA.* 106:15192–15197.
15. Bustamante, C., J. F. Marko, …, S. Smith. 1994. Entropic elasticity of lambda-phage DNA. *Science.* 265:1599–1600.
16. Gardel, M. L., J. H. Shin, …, D. A. Weitz. 2004. Elastic behavior of cross-linked and bundled actin networks. *Science.* 304:1301–1305.
17. Storm, C., J. J. Pastore, …, P. A. Janmey. 2005. Nonlinear elasticity in biological gels. *Nature.* 435:191–194.
18. Broedersz, C. P., and F. C. MacKintosh. 2011. Molecular motors stiffen non-affine semiflexible polymer networks. *Soft Matter.* 7:3186–3191.
19. Yao, N. Y., C. P. Broedersz, …, D. A. Weitz. 2013. Stress-enhanced gelation: a dynamic nonlinearity of elasticity. *Phys. Rev. Lett.* 110: 018103.
20. Sheinman, M., C. P. Broedersz, and F. C. MacKintosh. 2012. Actively stressed marginal networks. *Phys. Rev. Lett.* 109:238101.
21. Licup, A. J., S. Münster, …, F. C. MacKintosh. 2015. Stress controls the mechanics of collagen networks. *Proc. Natl. Acad. Sci. USA.* 112: 9573–9578.
22. Volokh, K. Y., O. Vilnay, and M. Belsky. 2000. Tensegrity architecture explains linear stiffening and predicts softening of living cells. *J. Biomech.* 33:1543–1549.
23. Fischer-Friedrich, E., A. A. Hyman, …, J. Helenius. 2014. Quantification of surface tension and internal pressure generated by single mitotic cells. *Sci. Rep.* 4:6213.
24. Stamenović, D., Z. Liang, …, N. Wang. 2002. Effect of the cytoskeletal prestress on the mechanical impedance of cultured airway smooth muscle cells. *J. Appl. Physiol.* 92:1443–1450.
25. Reymann, A.-C., F. Staniscia, …, S. W. Grill. 2016. Cortical flow aligns actin filaments to form a furrow. *eLife.* 5:e17807.
26. Prost, J., F. Jülicher, and J.-F. Joanny. 2015. Active gel physics. *Nat. Phys.* 11:111–117.
27. Landau, L., and E. Lifshitz. 1986. Theory of Elasticity, Third Edition. Elsevier, Amsterdam, Netherland.
28. Hoffman, B. D., G. Massiera, …, J. C. Crocker. 2006. The consensus mechanics of cultured mammalian cells. *Proc. Natl. Acad. Sci. USA.* 103:10259–10264.
29. Kollmannsberger, P., C. T. Mierke, and B. Fabry. 2011. Nonlinear viscoelasticity of adherent cells is controlled by cytoskeletal tension. *Soft Matter.* 7:3127–3132.
30. Schlosser, F., F. Rehfeldt, and C. F. Schmidt. 2015. Force fluctuations in three-dimensional suspended fibroblasts. *Philos. Trans. R. Soc. Lond. B Biol. Sci.* 370:20140028.
31. Trepat, X., G. Lenormand, and J. J. Fredberg. 2008. Universality in cell mechanics. *Soft Matter.* 4:1750–1759.

Biophysical Journal, Volume *114*

Supplemental Information

Active Prestress Leads to an Apparent Stiffening of Cells through Geometrical Effects

Elisabeth Fischer-Friedrich

I. GEOMETRICAL COUPLING WITH PHASE-SHIFTED, FREQUENCY-DEPENDENT ACTIVE FORCE CONTRIBUTIONS

In the first and second example in the main text, geometrical coupling of active prestress has contributed only a frequency-independent addition to the measured storage modulus of the system. In the following, we will present an example where geometrical coupling gives rise to a complex-valued, frequency-dependent addition to the effective elastic modulus of the system for the case of a deflected prestressed fibre with a viscoelastic connector between the bead and the fiber (see Fig. 1B, main text). The bead is deflected in a vertical manner. The combined system has a (complex) spring constant

$$k_{comb} = 1/(1/k_{conn} + 1/k_{fibre}),$$

where k_{conn} and k_{fibre} are the effective (complex) spring constants of the connector and the fibre with respect to vertical deflection. One finds

$$k_{fibre}(\sigma_{\rm act}, \omega) = 16h_0^4/(4h_0^2 + L^2)^{3/2} G^*_{\rm meas}(\sigma_{\rm act}, \omega),$$

where $G^*_{\rm meas}$ equals the r.h.s of formula (6), main text. Thus, in the stiffness of the combined system k_{comb}, the active term in $G^*_{\rm meas}$ contributes in general also to the imaginary part of the system and is frequency-dependent.

II. DETERMINING THE GEOMETRICAL FACTOR FOR THE CASE OF A DEFLECTED PRESTRESSED CYTOSKELETAL FIBRE

In the main text, we where discussing the example of geometrical coupling of active stress in a prestressed cytoskeletal fibre tethered at its end points at a distance L (see Fig. 1A, main text). Height oscillations are imposed on the fibre center with $h(t) = h_0 + \tilde{h}\exp(i\omega t)$. Here, we derive the factor of geometrical coupling $1/g_0 \cdot \tilde{g}/\tilde{\epsilon}$ for this specific example.

We make a perturbation calculation determining the fibre oscillation dynamics up to first order in height amplitude $\tilde{h}$. We make the following expansions of the dynamic fibre length $l(t)$ and the dynamic angle $\alpha(t)$ between the substrate and the fibre

$$\begin{aligned} l(t) &= l_0 + \tilde{l}\exp(i\omega t) + \mathcal{O}(\tilde{h}^2), \\ \alpha(t) &= \alpha_0 + \tilde{\alpha}\exp(i\omega t) + \mathcal{O}(\tilde{h}^2). \end{aligned}$$

Using the geometrical relations $\sin(\alpha(t)) = h(t)/(l(t)/2)$ and $h(t)/(L/2) = \tan(\alpha(t))$, we obtain

$$\begin{aligned} l_0 &= \sqrt{4h_0^2 + L^2}, \\ \alpha_0 &= \arctan(2h_0/L), \\ \tilde{\alpha} &= (2\tilde{h}L)/(4h_0^2 + L^2), \\ \tilde{l} &= (4h_0\tilde{h})/\sqrt{4h_0^2 + L^2}. \end{aligned} \tag{1}$$

We can thus calculate the time variation of the geometrical factor $g(t) = 2\sin(\alpha(t))$ to first order

$$\begin{aligned} g(t) &\equiv g_0 + \tilde{g}\exp(i\omega t) + \mathcal{O}(\tilde{h}^2) \\ &= 2\sin(\alpha_0) + 2\cos(\alpha_0)\tilde{\alpha}\exp(i\omega t) + \mathcal{O}(\tilde{h}^2) \\ &= \frac{2\tan(\alpha_0)}{\sqrt{1+\tan(\alpha_0^2)}} + \frac{2\tilde{\alpha}}{\sqrt{1+\tan(\alpha_0^2)}}\exp(i\omega t) + \mathcal{O}(\tilde{h}^2) \\ &= \frac{4h_0}{\sqrt{4h_0^2+L^2}} + \frac{4\tilde{h}L^2}{(4h_0^2+L^2)^{3/2}}\exp(i\omega t) + \mathcal{O}(\tilde{h}^2), \end{aligned}$$

where we have used Eqn. (1) in the last transformation step. We conclude that $g_0 = \frac{4h_0}{\sqrt{4h_0^2+L^2}}$ and $\tilde{g} = \frac{4\tilde{h}L^2}{(4h_0^2+L^2)^{3/2}}$. The strain amplitude of the fibre is $\tilde{\epsilon} = \tilde{l}/l_0$. We thus obtain the coupling geometrical factor as

$$\begin{aligned} \frac{1}{g_0}\frac{\tilde{g}}{\tilde{\epsilon}} &= \frac{1}{\frac{4h_0}{\sqrt{4h_0^2+L^2}}} \frac{\frac{4\tilde{h}L^2}{(4h_0^2+L^2)^{3/2}}}{\frac{\tilde{l}}{l_0}} \\ &= \frac{L^2}{4h_0^2}. \end{aligned}$$